Letter

Simulation Analysis of Deformation Control for Magnetic Soft Medical Robots

Jingxi Wang, Baoyu Liu, Edmond Q. Wu, *Senior Member, IEEE*, Jin Ma, and Ping Li, *Member, IEEE*

Dear Editor,

This letter presents a biocompatible cross-shaped magnetic soft robot and investigates its deformation mode control strategy through COMSOL modeling and simulation. Magnetic soft robots offer novel avenues for precise treatment within intricate regions of the human body. However, the biosafety and precise control characteristics of robots need to be further improved for practical medical use. In this study, a cross-shaped magnetic soft robot was designed based on biocompatible chitosan material. The cross-shaped magnetic soft robot exhibited programmable and controllable deformation behaviors by manipulating the external magnetic field and the composition of magnetic materials through the finite element method. The findings of this study provide support for the precise control of magnetic soft medical robots and offer insights for the design of programmable motion robots.

The treatment of intricate and delicate regions within the human body presents a challenge in clinical medicine. Robotic systems possess the capability to maneuver freely within the body, achieving precise deformations and movements through autonomous control. These robots can serve as minimally invasive or non-invasive tools to apply for various medical situations [1]−[3].

Related work: To date, various robotic systems have been researched for diverse medical scenarios [4], [5]. Soft robots based on hydrogel materials exhibit pliable characteristics that avoid harming human tissue. Moreover, these soft robots boast an infinite range of degrees of freedom. This endows them with stronger deformability and consequently more versatile motion characteristics compared to rigid robots [6]−[8]. Liu *et al.* [9] engineered a mechanically-driven bio-inspired frictional electro-soft robot capable of transmitting images within narrow tunnels for swift diagnostics. Wang *et al.* [10] fabricated an electromagnetic force-driven soft robot emulating kangaroo jumping motion across different surfaces.

In terms of driving mode, the magnetic field actuation makes the robots more convenient for the human environment. Its non-contact remote control feature renders magnetic soft robots particularly suitable for precision medical applications [11]. The deformation and motion of magnetic soft robots can be programmatically controlled. This enables functionalities such as grasping, enveloping, releasing of target objects, precise route planning, and traversal [12]. Moreover, magnetic soft robots exhibit rapid responsiveness to magnetic fields, thereby ensuring swift completion of medical procedures.

Corresponding authors: Jin Ma and Ping Li.

Citation: J. Wang, B. Liu, E. Wu, J. Ma, and P. Li, "Simulation analysis of deformation control for magnetic soft medical robots," *IEEE/CAA J. Autom. Sinica*, vol. 11, no. 3, pp. 794–796, Mar. 2024.

J. Wang, B. Liu, and P. Li are with Key Laboratory of Biomechanics and Mechanobiology (Beihang University), Ministry of Education Beijing Advanced Innovation Center for Biomedical Engineering, the School of Biological Science and Medical Engineering, Beihang University, Beijing, 100083, China (e-mail: wjingxi@buaa.edu.cn; lliubaoyu0214@buaa.edu.cn; liping@buaa.edu.cn).

E. Wu is with the Department of Automation, Shanghai Jiao Tong University, Shanghai 200240, China (e-mail: edmondqwu@sjtu.edu.cn).

J. Ma is with the Department of Aerospace Medicine, Air Force Medical University, Xi'an 710032, China (e-mail: 780216@fmmu.edu.cn).

Color versions of one or more of the figures in this paper are available online at http://ieeexplore.ieee.org.

Digital Object Identifier 10.1109/JAS.2023.124143

Consequently, magnetic soft robots can access intricate human body regions and execute precise treatments.

However, the robot systems applicable for practical medical use remain limited. As robot systems are intended for deployment within the human body, their safety must be meticulously considered. On one hand, materials for robots entering the human body must exhibit biocompatibility to mitigate potential immunological risks. Biocompatibility has not been fully considered in most of the existing research on robots.

On the other hand, the control and motion errors of magnetic soft robots must be maintained relatively small to achieve precise manipulation of programmed motion patterns. The modeling methods based on geometric models and mechanical models have achieved preliminary results in the research of soft robot motion [13]. Arachchige *et al.* [14] proposed a floating-base kinematic model with distributed contact dynamics and achieved locomotion gait trajectories for the soft robotic snakes. Although they have a good level of computational accuracy, the parameterization and implementation in the model are very complex, and the functionality is limited in the simulation and environmental contact problems. The finite element method provides a strategy for solving these above problems. The elastic matrix is calculated based on the constitutive relation of the materials measured by experiments, and the iterative method of model constraint is adopted. However, the finite element analysis based on biocompatible robots is not sufficient, which is difficult to be used for accurate robot control.

Hence, this letter presents the design of a magnetic soft robot based on biocompatible chitosan materials, and studied the motion modes based on finite element simulation COMSOL method. The robot's precise deformation and motion control characteristics are investigated based on the constitutive relation of biocompatible materials and finite element method for facilitating precision medicine.

Design and construction of magnetic soft robots: The design and preparation of magnetic soft robots with different magnetic properties were first carried out. Magnetic Fe_3O_4 nanoparticles with a diameter of about 9 nm were added into chitosan solution dissolved by alkaline reagents [15]. The mass fractions of magnetic Fe_3O_4 nanoparticles were 5%, 10%, 20%, 30%, and 40%. The mixed solution was poured into a designed mold and molded by heating at 60 ℃ to obtain magnetic soft robots of different shapes. In this work, the magnetic soft robot was designed in the shape of a cross. The mechanical and magnetic properties of the robot materials were measured for the characterization of the constitutive relations in the finite element simulation.

Modeling and simulation methods: A disc-shaped permanent magnet was used in this work as the driving magnetic field for the robot. According to Maxwell-Ampere's law, the following equation exists for the magnetic field of the permanent magnet:

$$\nabla \times \left(\frac{1}{\mu_0} B - M \right) = \nabla \times H = 0 \tag{1}$$

where ∇ is the gradient operator, μ_0 is the magnetic permeability in classical vacuum, B is the magnetic flux density, M is the magnetization, and H is the magnetic field strength.

In the spin-free field

$$H = -\nabla V_m \tag{2}$$

where V_m is the magnetic scale potential.

Gauss's magnetic law is

$$B = \mu_0(H + M). \tag{3}$$

Therefore, the static magnetic field equation for a permanent magnet is

$$-\nabla \cdot (\mu_0 (\nabla V_m + M)) = 0. \tag{4}$$

Magnetic soft robots are subjected to magnetic field force F and magnetic field torque T in a magnetic field. In a gradient magnetic field, the magnetic material experiences an inhomogeneous magnetic field and is subjected to the magnetic field force calculated as

$$F_{\text{robot}} = V_{\text{robot}}(M_{\text{robot}} \cdot \nabla)B \qquad (5)$$

where F_{robot} represents the magnetic force, V_{robot} denotes the volume of the magnetic soft robot, M_{robot} is the magnetization vector of the magnetic soft robot, and B signifies the magnetic flux density of the external magnetic field.

Therefore, the magnetic field force experienced by a magnetic soft robot is closely related to the properties of the magnetic material itself and the magnitude of the magnetic field gradient. In this work, the magnetic properties of the magnetic soft robots were changed by adjusting the concentration of magnetic nanoparticles. And the magnetic field gradient was changed by adjusting the positional relationship between the external permanent magnet and the robots.

When the magnetization direction of the magnetic material and the direction of the magnetic field strength do not coincide, the magnetic material will be subjected to the magnetic field torque. The magnetic field torque prompts the magnetization direction of the magnetic material to turn to the direction of the external magnetic field. The magnetic field torque formula is

$$T_{\text{robot}} = V_{\text{robot}} M_{\text{robot}} \times B \qquad (6)$$

where T_{robot} represents the magnetic field torque, V_{robot} denotes the volume of the magnetic soft robot, M_{robot} is the magnetization vector of the magnetic soft robot, and B signifies the magnetic flux density of the external magnetic field.

Utilizing the COMSOL multiphysics modeling software package (COMSOL, Inc.), modeling and multi-physics field simulations were conducted to analyze the deformation behaviors of a cross-shaped magnetic soft robot under different magnetic fields and combinations of magnetic materials. The analyses were performed using the AC/DC module and the structural mechanics module. Initially, both the cross-shaped magnetic soft robot and the permanent magnet were modeled. The robot consisted of four rectangular arms, each measuring 25 mm in length, 10 mm in width, and 1 mm in thickness; a non-magnetic square material with a side length of 10 mm occupied the center. The edges of the cross-shaped magnetic soft robot were composed of chitosan material with varying concentrations of magnetic nanoparticles (40%, 30%, 20%, 10% and 5%). The permanent magnet, a cylinder with a radius of 30 mm and height of 10 mm, was positioned directly above the robot's center. The "Zero Magnetic Scalar Potential" condition was applied as a boundary condition. The investigation focused on the motion control modes of the cross-shaped magnetic soft robot under different magnetic fields and material combinations.

Deformation patterns controlled by various magnetic fields: The analysis commenced with the study of deformation patterns of the cross-shaped magnetic soft robot under different magnetic fields. As depicted in Fig. 1, a cross-shaped magnetic soft robot composed of chitosan hydrogel with 40% magnetic Fe_3O_4 nanoparticle content exhibited displacement deformations at varying distances from the permanent magnet. The robot displayed pronounced symmetry. For each arm, from the inside out, deformation progressively increased. This phenomenon was linked to the magnetic field gradient, as the edges of the magnetic soft robot experienced the highest gradient at their endpoints. Furthermore, an analysis of the robot's deformation at different distances from the permanent magnet was conducted. At a distance of 45 mm, the robot displayed minimal deformation, attributed to the rapid decrease in magnetic field intensity and gradient further away from the permanent magnet. At distance of 40 mm and 35 mm, slight displacement occurred at the endpoints of the robot's four arms. However, as the cross-shaped magnetic soft robot approached the permanent magnet closely (30 mm), it exhibited pronounced deformation. This response resulted from the increasing magnetic field gradient. Notably, when positioned 30 mm away from the permanent magnet, the robot underwent significant deformation with substantial gradients along each arm's deformation. These observations collectively underscored the rapid increase in magnetic field gradient.

Furthermore, calculations of the maximum displacement of the cross-shaped magnetic soft robot at varying distances from the permanent magnet were performed, as depicted in Fig. 2. As the distance from the permanent magnet decreased, the maximum displacement of the cross-shaped magnetic soft robot increased. When positioned over 35 mm away from the permanent magnet, the robot's
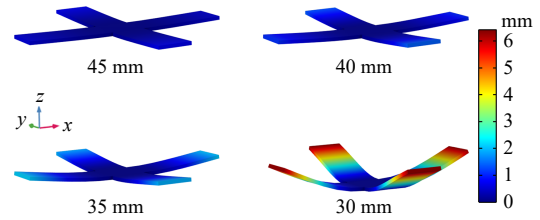

Fig. 1. Deformation patterns of the cross-shaped magnetic soft robot at different distances from the permanent magnet.
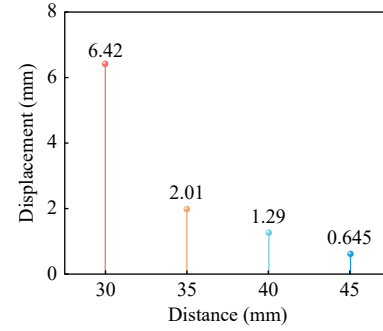

Fig. 2. Maximum displacement of the cross-shaped magnetic soft robot at different distances from the permanent magnet.

maximum displacement remains within 2 mm or below, indicating minimal deformation. However, at a distance of 30 mm from the permanent magnet, the robot's displacement reached 6.42 mm, showcasing substantial growth. Decreasing the distance from the permanent magnet resulted in an increased magnetic field gradient, thus subjecting the cross-shaped magnetic soft robot to a greater magnetic force for amplified displacement.

Consequently, a sufficiently significant magnetic field gradient became imperative when driving magnetic soft robots. Moreover, by controlling the distance between the magnetic soft robot and the permanent magnet, the magnetic field gradient can be manipulated, enabling diverse deformation behaviors in the magnetic soft robot. The exhibited enveloping deformation behavior of this cross-shaped magnetic soft robot lends itself to object encapsulation and transport. By regulating the external magnetic field, distinct deformation motion patterns can be achieved in the cross-shaped magnetic soft robot to accommodate diverse functional requirements.

Deformation patterns of different magnetic materials combinations: In addition to modifying the external magnetic field, diverse deformation motion patterns can also be generated in the cross-shaped magnetic soft robot through the design of various combinations of magnetic materials. The four arms of the cross-shaped magnetic soft robot were divided into two groups. Specifically, the two arms aligned in a straight line constituted one group. Among the two groups, one group of arms was composed of chitosan hydrogel with a fixed content of 40% magnetic Fe_3O_4 nanoparticles. The other group of arms was composed of chitosan hydrogel with varying contents of 5%, 10%, 20%, or 30% magnetic Fe_3O_4 nanoparticles. The distance between the permanent magnet and the cross-shaped magnetic soft robot was fixed at 30 mm. The deformation behaviors of the cross-shaped magnetic soft robots with different combinations of magnetic materials were investigated, as depicted in Fig. 3. The robots exhibited noticeable symmetry, with consistent deformation behaviors in the two arms of each group. When the cross-shaped magnetic soft robot was composed of 5% and 40% magnetic material combinations, substantial discrepancies in deformation were evident between the two arm groups. The arms composed of 5% magnetic material exhibited minimal deformation, while those composed of 40% magnetic material demonstrated significant deformation. Furthermore, with an increase in the concentration of magnetic material to 10%, the deformation of the cross-shaped magnetic soft robot intensified. When the concentration of magnetic material rose to 20% and 30%, the divergence in deformation behaviors between the two arm groups
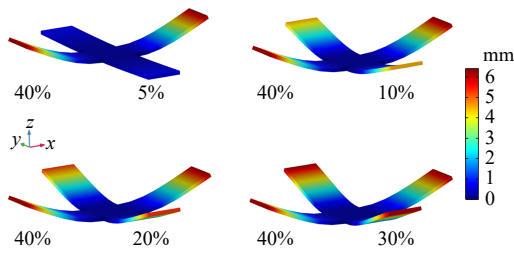
Fig. 3. Deformation patterns of the cross-shaped magnetic soft robots with different magnetic materials.

diminished. This observation aligned with the calculated formula for magnetic force. The arm composed of 5% magnetic nanoparticles experienced the smallest magnetic force and consequently exhibited the least deformation. As the concentration of magnetic nanoparticles grew, the magnetic force amplified. It resulted in greater deformation. The design of different combinations of magnetic materials facilitates the generation of diverse deformation motion patterns for the robots.

Furthermore, an analysis of the displacement distribution along the central line of the cross-shaped magnetic soft robots with different magnetic materials was conducted as illustrated in Fig. 4. Starting from one side of the cross-shaped magnetic soft robot, the displacement gradually diminished with an increase in robot length. Upon reaching the middle of the robot, the displacement reduced to zero. Subsequently, upon traversing to the other side of the cross-shaped magnetic soft robot, the displacement began to increase, culminating in the maximum displacement at the endpoints of the robot's arms. Corresponding with Fig. 3, higher concentrations of magnetic nanoparticles led to larger displacements in the cross-shaped magnetic soft robot. When the concentration of magnetic nanoparticles was too low, the cross-shaped magnetic soft robot lacked the necessary magnetic force to induce effective deformation motion.
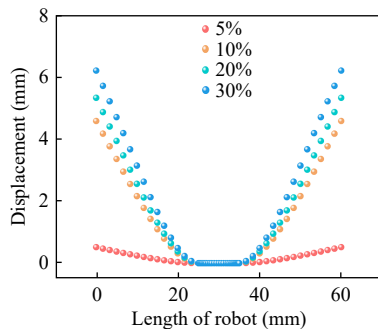

Fig. 4. Displacement distribution along the central line of the cross-shaped magnetic soft robots with different magnetic materials.

By increasing the concentration of magnetic nanoparticles, the deformation of the cross-shaped magnetic soft robot can be enhanced. Furthermore, distinct deformation displacements corresponded to different concentrations of magnetic nanoparticles. Through the combination design of robot shape and materials, a more diverse array of deformation patterns can be achieved. This study solely presents simplified combinations of the cross-shaped magnetic soft robot. Through the utilization of multi-gradient combinations and designs, the robot can exhibit a broader range of deformation behaviors, such as serpentine, fish-like, and jellyfish-like motions. This design can achieve precise control of motion patterns.

Conclusions: This study presents a cross-shaped magnetic soft robot designed with biocompatible chitosan materials and employs COMSOL simulations to investigate its deformation control modes. The simulation results demonstrated that external magnetic field conditions could effectively govern the deformation displacement of the cross-shaped magnetic soft robot. Furthermore, by designing and combining magnetic materials with different magnetic characteristics, the cross-shaped magnetic soft robot could manifest diverse internal deformation behaviors for motion pattern control. Therefore, this cross-shaped magnetic soft robot lays a foundational theoretical groundwork for precise medical applications. For the simulation method, more elaborate modeling and calculation optimization are required to improve the simulation accuracy and reduce the calculation amount. In the future, the optimization of robot and simulation parameters through practical experiments will be necessary to meet the demands of precise medical applications.

References

[1] X. Du and J. Yu, "Image-integrated magnetic actuation systems for localization and remote actuation of medical miniature robots: A survey," *IEEE Trans. Robotics*, vol. 39, no. 4, pp. 2549–2568, 2023.

[2] S. Hans and F. O. M. Joseph, "Robust control of a bevel-tip needle for medical interventional procedures," *IEEE/CAA J. Autom. Sinica*, vol. 7, no. 1, pp. 244–256, 2019.

[3] S. Ling, H. Wang, and P. Liu, "Adaptive fuzzy dynamic surface control of flexible-joint robot systems with input saturation," *IEEE/CAA J. Autom. Sinica*, vol. 6, no. 1, pp. 97–107, 2019.

[4] F. Xu and H. Wang, "Soft robotics: Morphology and morphology-inspired motion strategy," *IEEE/CAA J. Autom. Sinica*, vol. 8, no. 9, pp. 1500–1522, 2021.

[5] H. Wang, M. Totaro, and L. Beccai, "Toward perceptive soft robots: Progress and challenges," *Advanced Science*, vol. 5, no. 9, p. 1800541, 2018.

[6] D. Li, Y. Zhang, P. Li, R. Law, Z. Xiang, X. Xu, L. Zhu, and E. Wu, "Position errors and interference prediction-based trajectory tracking for snake robots," *IEEE/CAA J. Autom. Sinica*, vol. 10, no. 9, pp. 1810–1821, 2023.

[7] A. H. Khan, Z. Shao, S. Li, Q. Wang, and N. Guan, "Which is the best PID variant for pneumatic soft robots an experimental study," *IEEE/CAA J. Autom. Sinica*, vol. 7, no. 2, p. 451, 2020.

[8] D. Zhang, H. Yuan, and Z. Cao, "Environmental adaptive control of a snake-like robot with variable stiffness actuators," *IEEE/CAA J. Autom. Sinica*, vol. 7, no. 3, pp. 745–751, 2020.

[9] Y. Liu, B. Chen, W. Li, L. Zu, W. Tang, and Z. Wang, "Bioinspired triboelectric soft robot driven by mechanical energy," *Advanced Functional Materials*, vol. 31, no. 38, p. 2104770, 2021.

[10] Q. Wang, X. Lu, N. Yuan, and J. Ding, "Small-scale soft robot with high speed and load capacity inspired by Kangaroo hopping," *Advanced Intelligent Systems*, vol. 4, no. 1, p. 2100129, 2022.

[11] Y. Xu, K. Li, Z. Zhao, and M. Q.-H. Meng, "A novel system for closed-loop simultaneous magnetic actuation and localization of WCE based on external sensors and rotating actuation," *IEEE Trans. Autom. Science and Engineering*, vol. 18, no. 4, pp. 1640–1652, 2020.

[12] Y. Kim and X. Zhao, "Magnetic soft materials and robots," *Chemical Reviews*, vol. 122, no. 5, pp. 5317–5364, 2022.

[13] O. Yasa, Y. Toshimitsu, M. Y. Michelis, L. S. Jones, M. Filippi, T. Buchner, and R. K. Katzschmann, "An overview of soft robotics," *Annual Review of Control, Robotics, and Autonomous Systems*, vol. 6, pp. 1–29, 2023.

[14] D. D. Arachchige, S. Mallikarachchi, I. Kanj, D. M. Perera, Y. Chen, H. B. Gilbert, and I. S. Godage, "Dynamic modeling and validation of soft robotic snake locomotion", in *Proc. 9th Int. Conf. Control, Automation and Robotics*, 2023, pp. 6–12.

[15] J. Wang, K. Li, J. Xu, M. Liu, P. Li, X. Li, and Y. Fan, "A biomimetic hierarchical small intestinal submucosa–chitosan sponge/chitosan hydrogel scaffold with a Micro/Nano structure for dural repair," *J. Materials Chemistry B*, vol. 9, no. 37, pp. 7821–7834, 2021.